Local structure in $BaTi_{1-x}Zr_xO_3$ relaxors from neutron pair distribution function analysis

C. Laulhé,[1] F. Hippert,[1] R. Bellissent,[2] A. Simon,[3] and G. J. Cuello[4]
[1]*Laboratoire des Matériaux et du Génie Physique (CNRS-Grenoble INP), MINATEC, 3 parvis Louis Néel, B. P. 257, F-38016 Grenoble Cedex 01, France*
[2]*CEA Grenoble, INAC/SPSMS, 17 rue des Martyrs, F-38054 Grenoble Cedex 9, France*
[3]*Institut de Chimie de la Matière Condensée de Bordeaux, CNRS, 87 avenue A. Schweitzer, F-33608 Pessac, France*
[4]*Institut Laue-Langevin, 6 rue Jules Horowitz, B. P. 156, F-38042 Grenoble Cedex 9, France*
(Received 5 June 2008; published 9 February 2009)

The pair distribution functions (PDF) of $BaTi_{1-x}Zr_xO_3$ (BTZ) relaxors ($x=0.25, 0.32, 0.35$), as well as those of the end members $BaTiO_3$ and $BaZrO_3$, were determined at 300 K from neutron powder scattering data. In the relaxors, the PDF provides direct evidence that the Ti and Zr atoms do not occupy the equivalent octahedral sites expected from the crystallographic cubic perovskite structure. It is shown that the TiO_6 and ZrO_6 octahedra in BTZ relaxors are instead similar to those observed in $BaTiO_3$ and $BaZrO_3$, respectively. In $BaZrO_3$, the Zr atoms lie at the center of regular oxygen octahedra, forming nonpolar ZrO_6 units. In the tetragonal ferroelectric phase of $BaTiO_3$, the distribution of Ti-O distances within TiO_6 octahedra is found compatible with a displacement of the Ti atoms in the $[111]_p$ direction of the pseudocubic perovskite cell. We conclude that the local polarization in BTZ relaxors is mainly due to the displacements of the Ti atoms and that moreover the Ti displacements are very similar in BTZ relaxors and in the classical ferroelectric $BaTiO_3$.

DOI: 10.1103/PhysRevB.79.064104 PACS number(s): 77.84.Dy, 61.05.fg, 77.90.+k, 77.80.−e

I. INTRODUCTION

Relaxor ferroelectrics ("relaxors") form a fascinating class among ferroelectrics, which has aroused a wide range of experimental and theoretical investigations (see for instance Refs. 1–3). These materials are characterized by a broad and frequency-dependent maximum of the dielectric permittivity as a function of temperature, rather than the sharp and frequency-independent anomaly found in classical ferroelectrics. The peculiar properties of relaxors are generally related to the presence of randomly orientated polar nanoregions. However, the determination of their exact structural nature still represents an experimental challenge.[4]

Most relaxors crystallize in the ABO_3 perovskite structure, in which corner-linked oxygen octahedra define octahedral and cubo-octahedral sites (so-called *B* sites and *A* sites, respectively). If present, the polarization arises from displacements of *A* and/or *B* cations within their oxygen cages. In a classical ferroelectric, all the cation displacements share at least one common component, giving rise to a macroscopic polarization. In relaxors, the cation displacements are correlated or partially correlated on limited length scales only (20–100 nm) within the polar nanoregions, leading to a null macroscopic polarization.

In the present work, we focus on the $BaTi_{1-x}Zr_xO_3$ (BTZ) solid solution, which exhibits relaxor properties for $0.25 \leq x \leq 0.50$ (Ref. 5). One end member of the BTZ solid solution is the well-known classical ferroelectric $BaTiO_3$, which shows three different phases below the critical temperature $T_c=393$ K (Ref. 6 and references therein): (i) a rhombohedral one (space group $R3m$) between 0 and 183 K, due to displacements of the Ti and Ba atoms in the $[111]_p$ direction of the pseudocubic perovskite cell, (ii) an orthorhombic one ($Amm2$) between 183 and 278 K, due to average displacements of the Ti and Ba atoms in the $[110]_p$ direction, and (iii) a tetragonal one ($P4mm$) between 278 and 393 K, due to average displacements of the Ti and Ba atoms in the $[001]_p$ direction. Above T_c, $BaTiO_3$ has a nonpolar, cubic structure (space group $Pm\bar{3}m$), with null average cation displacements. Note that in all the phases of $BaTiO_3$ except the rhombohedral one, the local structure differs from the crystallographic structure, as evidenced by the presence of diffuse scattering[7,8] and confirmed by other experimental probes such as nuclear magnetic resonance (NMR) (Refs. 9 and 10) and x-ray absorption.[11] The other end member of the BTZ solid solution $BaZrO_3$ is paraelectric (neither Ba or Zr atoms are displaced) and cubic ($Pm\bar{3}m$) between 2 and 1675 K (Refs. 12–14). In this compound, the local structure is considered to be identical to the cubic crystallographic structure, as suggested by both NMR (Refs. 15 and 16) and x-ray absorption experiments.[17–21] It is interesting to note that the unit-cell volumes of $BaTiO_3$ and $BaZrO_3$ (64.270 and 73.665 Å^3 at 300 K, respectively) strongly differ, which is due to the difference between the Ti^{4+} and Zr^{4+} ionic radii (0.605 and 0.72 Å, respectively[22]). In the *x* range of interest for relaxor behavior ($0.25 \leq x \leq 0.50$), the structure of $BaTi_{1-x}Zr_xO_3$ at 300 K is the nonpolar, cubic $Pm\bar{3}m$ perovskite structure.[23] The cell volume linearly increases with *x*, according to Vegard's law expected from the unit-cell volumes of $BaTiO_3$ and $BaZrO_3$.[23] The crystallographic structure of BTZ relaxors is not expected to change with temperature since the dielectric anomaly does not mark any structural phase transition in relaxors.[1] Indeed, $BaTi_{0.65}Zr_{0.35}O_3$ remains cubic in the temperature range [80–300 K] (Ref. 24) that includes the temperature of the dielectric anomaly (~200 K, see Ref. 5).

All perovskite relaxors share two characteristics: (i) the presence of at least one ferroelectrically active cation (Pb^{2+}, Bi^{3+}, Ti^{4+}, or Nb^{5+}) and (ii) a chemical substitution on either the *A* or *B* site. The "Pb-based" relaxors, which are the most studied, present Pb^{2+} cations on the *A* site and an aliovalent substitution on the *B* site (e.g., Mg^{2+} and Nb^{5+} in the canoni-

cal relaxor $PbMg_{1/3}Nb_{2/3}O_3$). In that case, the composition fluctuations on the *B* site induce a charge disorder, which is thought to hinder the establishment of long-range ferroelectric correlations.[25] On the other hand, the "$BaTiO_3$-based" relaxor $BaTi_{1-x}Zr_xO_3$ exhibits an isovalent Ti^{4+}/Zr^{4+} substitution and hence, a much reduced charge disorder if any. In such a case, it can be proposed that the large difference between the Ti^{4+} and Zr^{4+} ionic radii generates structural distortions, which then impede the long-range ferroelectric arrangement of the cations (see Ref. 26 and references therein). However, the exact mechanism involved remains an open question.

The analysis of the Bragg peaks in BTZ relaxors reveals a cubic crystallographic structure, in which the Ti and Zr atoms lie at the center of identical, regular octahedra. Due to the assumption of periodicity underlying this analysis, the structural distortions and cation displacements expected in BTZ relaxors are averaged to zero. The aim of the present work is to describe these two structural features by studying the local structure in BTZ relaxors. For this purpose, one can analyze the pair distribution function (PDF), which is a histogram of all the interatomic distances present in a sample, each pair of atoms giving rise to a peak weighted by the product of their scattering powers.[27] The PDF can be obtained as the Fourier transform (FT) of the x-ray or neutron normalized total scattered intensity. In the case of crystalline samples, the scattered intensity is a superposition of Bragg peaks related to the periodic structure, and diffuse scattering related to distortions with respect to this average periodic structure. Making the FT of both the Bragg contributions and the diffuse scattering thus allows to probe the local structure. In particular, the PDF analysis has been successfully applied to determine the local cation displacements in ferroelectric perovskites beyond the average information given by crystallography.[28–36] Let us mention that the continuous development of PDF refinement programs[37,38] has extended this technique to the analysis of medium-range structures.

In the following, the PDFs obtained from neutron-scattering data are presented for three BTZ relaxors ($x=0.25, 0.32, 0.35$), as well as for the end-member compounds $BaTiO_3$ and $BaZrO_3$. Note that neutron scattering is particularly suited to study the BTZ relaxors. Indeed, due to the opposite signs of the Ti and Zr neutron coherent scattering lengths ($\bar{b}_{Ti}=-3.30$ fm and $\bar{b}_{Zr}=7.16$ fm), the contributions of pairs involving Ti and Zr atoms show up with opposite signs on the PDFs, emphasizing any difference between the local structure around these two atoms. In a first step, the experimental PDFs of $BaZrO_3$, $BaTiO_3$, and BTZ relaxors are compared with the PDFs calculated from their crystallographic structures in order to highlight the local structural distortions (Sec. III A). In a second step, we establish a link between the TiO_6/ZrO_6 octahedra present in BTZ relaxors and those present in the end-member compounds $BaTiO_3/BaZrO_3$ (Sec. III B). We finally propose a quantitative description of the TiO_6 and ZrO_6 octahedral units (Sec. IV) before discussing its implications on the relaxor behavior of BTZ (Sec. V).

II. EXPERIMENT

$BaTi_{1-x}Zr_xO_3$ ($x=0$, 0.25, 0.32, 0.35, and 1) powders were synthesized by solid-state reaction, starting from the appropriate amounts of $BaCO_3$, TiO_2, and ZrO_2 powders and following the method described in Ref. 5. X-ray diffraction patterns measured at 300 K allowed us to establish the single-phase character of all the synthesized powders. The barium titanate was found to be tetragonal with $a=3.992(2)$ Å and $c=4.033(2)$ Å, in agreement with previous reports.[6] The BTZ relaxors and the barium zirconate were found to be cubic, with $a=4.054(1)$, 4.067(1), 4.072(1), and 4.192(1) Å for $x=0.25$, 0.32, 0.35 and 1, respectively. The latter values are in good agreement with those previously published.[12,13,23]

The total scattered intensity was measured as a function of the scattering angle 2θ on the two-axes diffractometer D4 (Ref. 39) at the high-flux reactor at the Laue-Langevin Institute (ILL) for an incident neutron wavelength $\lambda=0.5$ Å. The angular range is $1.8\leq 2\theta\leq 137.2°$ with a 2θ step equal to 0.125°. The range of accessible neutron momentum transfer Q (with $Q=(4\pi \sin\theta)/\lambda$) extends therefore from 0.4 $Å^{-1}$ up to $Q_{max}=23.4$ $Å^{-1}$. All experiments were performed at 300 K. The powders (mass of about 10 g) were put into vanadium cylinders with an inner diameter of 8 mm. The Q resolution of the D4 diffractometer was deduced from the analysis of the scattered intensity of $BaZrO_3$ at 300 K. The profile of the measured diffraction peaks can be well approximated by a pseudo-Voigt function with a full width at half maximum varying according to $\Gamma_{instr}=0.12+5\times10^{-4}Q^2+5.2\times10^{-6}Q^4$, with Γ_{instr} and Q in $Å^{-1}$. This procedure is justified since the intrinsic width of the Bragg peaks of $BaZrO_3$, measured on a high-resolution x-ray diffractometer, does not exceed 0.01 $Å^{-1}$.

For each sample, the scattered intensity was obtained from the raw data by subtracting the empty container and sample environment contributions, taking into account absorption effects.[40] A standard multiple-scattering correction was applied.[41] Then, the intensities were corrected for the departures from the static approximation[42] (Placzeck correction). Due to the weakness of the neutron scattering and absorption cross sections in BTZ, the corrections for absorption and multiple-scattering effects are small: they do not exceed a few percent of the raw signal. On the contrary, the Placzeck correction is essential to get reliable scattered intensities. Finally, the incoherent-scattering contribution was subtracted in order to get the coherent scattering, and the data were normalized. The neutron-scattering length values were taken from Ref. 43. The resulting function is the so-called normalized coherent static scattering function, denoted $S(Q)$, which tends to 1 at large Q values. The $S(Q)$ obtained for $BaTiO_3$, $BaZrO_3$, and BTZ relaxors at 300 K are shown in Fig. 1.

The PDF, denoted $g(r)$ in the following, can be expressed as a function of all the interatomic distances present in the sample:[27]

$$4\pi r^2 g(r) = \frac{1}{N\bar{b}^2\rho_0}\sum_{\alpha,\beta}^{n}\overline{b_\alpha b_\beta}\sum_{\substack{i_\alpha,i_\beta \\ i_\alpha\neq i_\beta}}^{N_\alpha,N_\beta}\langle\delta(r-|\vec{r_{i_\alpha}}-\vec{r_{i_\beta}}|)\rangle, \quad (1)$$

where N represents the total number of atoms and n the number of different elements α in the studied sample. $\bar{b}_\alpha$ is the coherent scattering length of a particular element α and

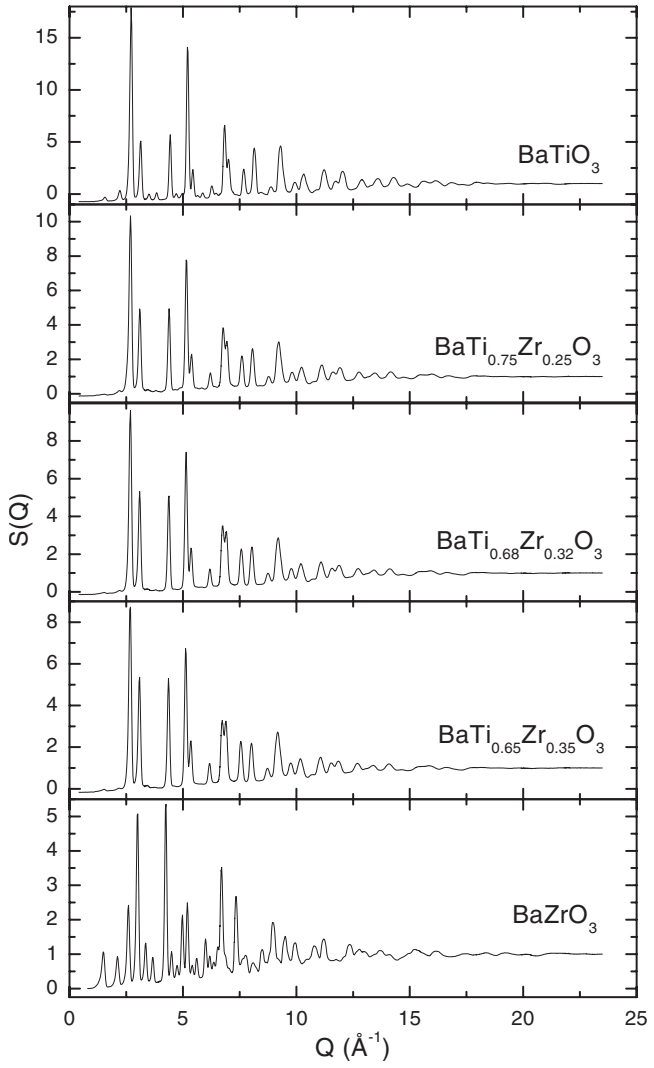

FIG. 1. Coherent static scattering functions of $BaTi_{1-x}Zr_xO_3$ (x=0, 0.25, 0.32, 0.35, and 1) at 300 K.

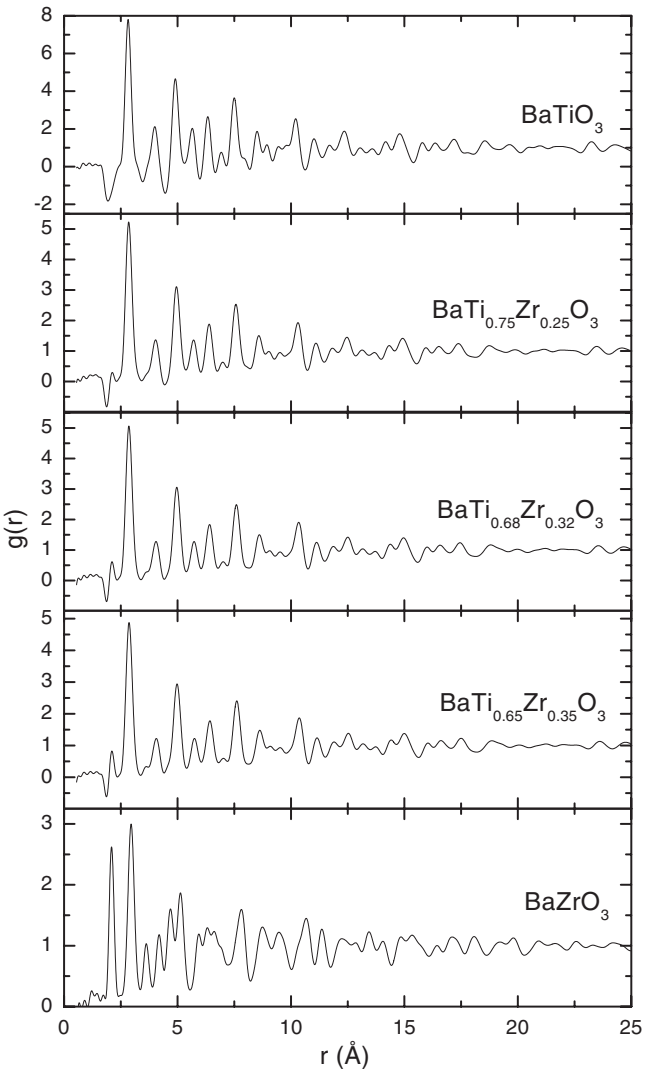

FIG. 2. Experimental pair distribution functions of $BaTi_{1-x}Zr_xO_3$ (x=0, 0.25, 0.32, 0.35, and 1) at 300 K.

$\bar{b}=\Sigma_\alpha^n c_\alpha \overline{b_\alpha}$ is the mean neutron-scattering length of the studied sample, averaged over all elements, each in atomic concentration $c_\alpha=N_\alpha/N$. ρ_0 is the atomic number density. $\vec{r}_{i_\alpha}$ is the position of the i_αth atom of nature α ($0\leq i_\alpha \leq N_\alpha$). The brackets $\langle\ \rangle$ stand for the average over all the atomic configurations that are accessible through thermal motion. The PDF is linked to the coherent static scattering function $S(Q)$ by the following FT relations:

$$S(Q)-1=\frac{4\pi\rho_0}{Q}\int_0^{+\infty} r[g(r)-1]\sin(Qr)dr, \qquad (2)$$

$$g(r)-1=\frac{1}{2\pi^2 r\rho_0}\int_0^{+\infty} Q[S(Q)-1]\sin(Qr)dQ. \qquad (3)$$

The latter equation makes possible the determination of the experimental PDF from the measured scattered intensity. The FT of $[S(Q)-1]$ was performed in the limited Q range [0.4–23.4 Å^{-1}] imposed by the diffractometer, which leads to spurious oscillations on both sides of each PDF peak. In order to reduce their magnitude, we multiplied $[S(Q)-1]$ by $e^{-(3/2)(Q/Q_{\max})^2}$ before the FT.[44] The $g(r)$ functions obtained for $BaTiO_3$, $BaZrO_3$, and BTZ relaxors at 300 K are presented in Fig. 2.

III. LOCAL STRUCTURE IN $BaTi_{1-x}Zr_xO_3$

A. Comparison between local and crystallographic structures

In order to evidence differences between the local and average structures, the experimental PDFs can be compared with those calculated from the crystallographic structures. We determine the calculated PDFs in three steps. First, the ideal PDF is calculated from a list of equilibrium positions by using Eq. (1), thermal motions being modeled by Gaussian distributions of the interatomic distances around their equilibrium values. Its inverse FT is then calculated according to Eq. (2), and convoluated with a pseudo-Voigt function whose full width at half maximum depends on Q (Sec. II). The result $S_{\text{calc}}(Q)$ can be compared to the measured $S(Q)$.

Finally, the calculated PDF $g_{calc}(r)$ is obtained by a FT of $S_{calc}(Q)$ using Eq. (3), the Q range and weight function being the same as for the experimental data (Sec. II). This calculation method allows to take properly into account the thermal motions in r space, as well as the instrument resolution function and the weight function used in Q space.

We calculated the PDFs from atomic clusters representative of the crystallographic structures of $BaZrO_3$, $BaTiO_3$, and BTZ relaxors at 300 K obtained from diffraction experiments.[6,13,23] The used cell parameters are those reported in Sec. II. The thermal motions are assumed to lead to a Gaussian distribution of the $i_\alpha - i_\beta$ interatomic distances around their equilibrium values $r_{i_\alpha i_\beta}$. The mean-square deviation is supposed to depend only on the elements α and β that constitute the pair, and on the $r_{i_\alpha i_\beta}$ distance: it is hence denoted $\sigma^2_{\alpha\beta}(r)$. We assumed the following dependence:[45]

$$\sigma^2_{\alpha\beta}(r) = \sigma^2_\alpha[1 - e^{-r/\delta_\alpha}]^2 + \sigma^2_\beta[1 - e^{-r/\delta_\beta}]^2. \quad (4)$$

In this equation, two parameters per element α are involved: (i) σ^2_α, the mean-square deviation of one component of an α atom displacement from its equilibrium position (assuming isotropic displacements), and (ii) a positive real number δ_α that allows to adjust the evolution of $\sigma^2_{\alpha\beta}(r)$ with r. The σ^2_α values for $BaTiO_3$ (σ^2_{Ba}=0.0031 Å^2, σ^2_{Ti}=0.0053 Å^2, σ^2_O =0.0051 Å^2) and $BaZrO_3$ (σ^2_{Ba}=0.0086 Å^2, σ^2_{Zr} =0.0058 Å^2, σ^2_O=0.0109 Å^2) were deduced from the diffraction analyses reported in Refs. 6 and 13. For the BTZ relaxors, the σ^2_{Ti} and σ^2_{Zr} parameters were set equal to their values in $BaTiO_3$ and $BaZrO_3$, respectively, and the σ^2_{Ba} and σ^2_O parameters were taken as the weighted sum of their values in $BaTiO_3$ and in $BaZrO_3$. For $BaZrO_3$, the δ_α coefficients were chosen in such a way that the mean-square deviations of the nearest-neighbor pair lengths Zr-O (2.096 Å), Zr-Ba (3.360 Å), and Zr-Zr (4.192 Å) are consistent with those deduced from extended x-ray absorption fine structure (EXAFS) data at the Zr K edge.[20] We used the following values: δ_{Ba}=2.4, δ_{Zr}=4.0, and δ_O=2.7. Due to the absence of a similar information for $BaTiO_3$ and BTZ relaxors, we simply assumed that the δ_{Ba}, δ_{Zr}, and δ_O parameters keep the same values as in $BaZrO_3$, and that $\delta_{Ti} = \delta_{Zr}$.

From the calculated PDFs, we determined the r ranges associated with each atomic pairs inside the pseudocubic perovskite unit cell. For r values ranging from 1.65 to 2.40 Å, only the Ti-O and/or Zr-O pairs inside the TiO_6 and ZrO_6 octahedra contribute to the PDFs. The peak observed in the r range [2.50–3.15 Å] is due to the O-O pairs forming the octahedral and cubo-octahedral cage edges, as well as to the Ba-O distances within the cubo-octahedra. The modulation of the PDFs in the r range [3.20–3.70 Å] corresponds to the Ba-Ti and/or Ba-Zr distances. The peak observed in the r range [3.70–4.40 Å] contains the contribution of all the pairs with an interatomic distance close to the pseudocubic cell parameter of the perovskite structure (Ba-Ba, O-O, Ti-Ti and/or Zr-Zr, and/or Ti-Zr).

The experimental PDF of $BaZrO_3$ at 300 K is compared with the calculated one in Fig. 3(a). In this compound, no noticeable deviations from the crystallographic $Pm\bar{3}m$ perovskite structure are expected:[15–21] therefore, the calculated and experimental PDFs should be identical. Indeed, in all the accessible r range [0–25 Å], the positions of the calculated and experimental peaks coincide within the experimental accuracy (0.01 Å). The observed differences in the amplitude and width of a few peaks are due to the approximations made to describe the thermal motions: r dependence of $\sigma^2_{\alpha\beta}(r)$ given by Eq. (4) and hypothesis of isotropic displacements. Therefore, they can be taken as a quantitative estimation of the uncertainties related to the experiment and to the model used to describe thermal motions.

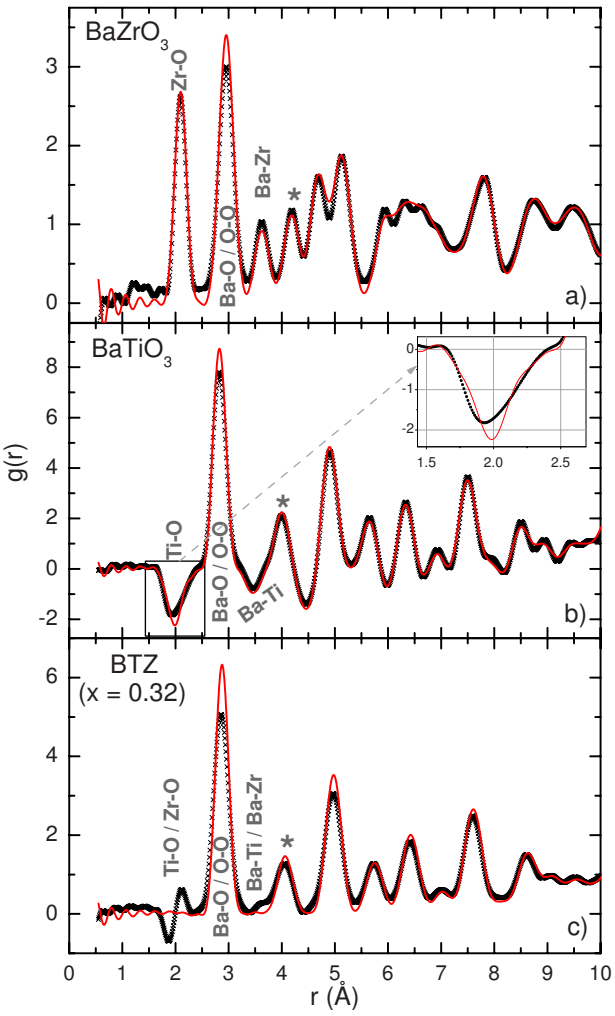

FIG. 3. (Color online) Experimental pair distribution function of (a) $BaZrO_3$, (b) $BaTiO_3$, and (c) $BaTi_{0.68}Zr_{0.32}O_3$ at 300 K (crosses), compared with the PDF calculated from their crystallographic structures (lines). Inset in figure (b): zoom on the contribution of the Ti-O pairs within the TiO_6 octahedra in $BaTiO_3$. On each graph, the first four peaks are identified, the * symbol representing peaks related to Ba-Ba, O-O, Ti-Ti and/or Zr-Zr, and/or Ti-Zr pairs. The r range [0–1.6 Å] is dominated by spurious oscillations due to the FT procedures and should not be considered in the comparisons.

The experimental PDF of $BaTiO_3$ at 300 K is compared with the calculated one in Fig. 3(b). In that case, the interatomic distances deduced from the crystallographic tetragonal structure are expected to differ from those observed on the short- and medium-range scales (see Sec. I). Surprisingly, the calculated and experimental PDFs only differ at small r

values. In the r range that corresponds to the Ti-O distances within the TiO_6 octahedra, one can clearly see that the calculated and experimental contributions exhibit different shapes and maxima positions [inset of Fig. 3(b)]. For r values larger than 3.15 Å, an excellent agreement is observed. Hence, the experimental PDF of $BaTiO_3$ does not allow to detect deviations of the atomic positions with respect to those described by the crystallographic tetragonal structure, except for the Ti and O atoms within the TiO_6 octahedra. In Sec. IV B, the experimental distribution of Ti-O distances at 300 K will be further analyzed within the framework of the displacive and order-disorder models for the phase transitions in $BaTiO_3$.

The experimental PDF of the relaxor $BaTi_{0.68}Zr_{0.32}O_3$ is compared with the PDF calculated from its cubic $Pm\bar{3}m$ crystallographic structure in Fig. 3(c). For the calculated PDF, the Zr and Ti atoms that share the B site were modeled by a single mean atom, characterized by the scattering length $(1-x)\overline{b_{Ti}}+x\overline{b_{Zr}}$. For $x=0.32$, the neutron-scattering length of the mean atom is equal to 0.047 fm, which is nearly zero. As a consequence, all the peaks that involve the mean atom are absent from the calculated PDF: in particular, no contribution is observed in the r range [1.65–2.40 Å] that corresponds to the (Ti,Zr)-O distances within the octahedra. On the contrary, the experimental PDF shows large variations in this range, with a negative contribution at low r values (1.7–2.0 Å), and a positive one at higher r values (2.0–2.4 Å). This simple observation proves that the oxygen environments of the Ti and Zr atoms are not equivalent, which could result from different shapes of the O_6 cages around Ti and Zr atoms, and/or different displacements of the Ti and Zr atoms within their octahedra. Moreover, the relative positions of the PDF contributions indicate the existence of Ti-O distances that are shorter than the Zr-O ones. For r values larger than 2.4 Å, the observed small differences between the experimental and calculated PDFs are less easy to interpret. Similar conclusions are obtained for $BaTi_{0.75}Zr_{0.25}O_3$ and $BaTi_{0.65}Zr_{0.35}O_3$ relaxors.

In summary, the comparison of the experimental PDFs of BTZ relaxors with the PDFs calculated from their crystallographic structures shows that the most striking differences occur in the r range corresponding to the (Ti/Zr)-O distances. Since the Ti-O and Zr-O distance distributions are related to the structure of the TiO_6 and ZrO_6 octahedra, we expect that the latter differences contain interesting information on both the O_6 cage deformations and eventual Ti/Zr off centering.

B. Comparison of the PDFs in BTZ relaxors and the PDFs in $BaTiO_3$ and $BaZrO_3$

In Sec. III A, we showed that the Ti and Zr atoms cannot be treated as a single mean atom in BTZ relaxors, some of the Ti-O distances being shorter than the Zr-O ones. In the present section, we test the opposite hypothesis: we assume that the Ti (Zr) oxygen environment in BTZ relaxors is the same as in $BaTiO_3$ ($BaZrO_3$). For that purpose, the weighted sum of the experimental PDFs of $BaTiO_3$ and $BaZrO_3$, denoted $g_x(r)$, is considered. The PDFs being normalized by the product $[\rho_0\bar{b}^2]$ for each sample [Eq. (1)], one has

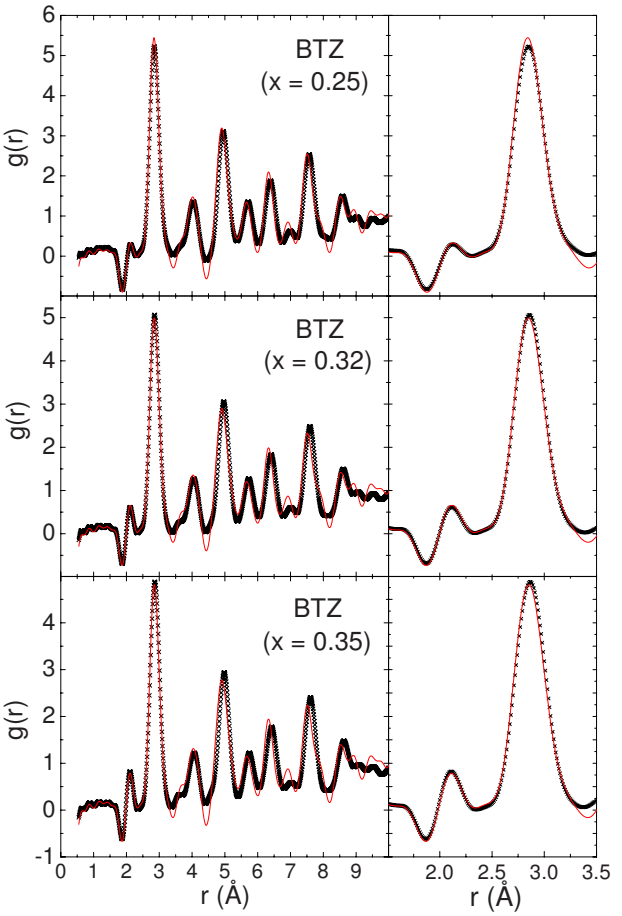

FIG. 4. (Color online) (left) Experimental pair distribution functions of $BaTi_{1-x}Zr_xO_3$ ($x=0.25,0.32,0.35$) at 300 K (crosses), compared with the weighted sums $g_x(r)$ of the experimental PDFs of $BaTiO_3$ and $BaZrO_3$ at 300 K (line); see Eq. (5). (right) Zoom in the r range [1.5–3.5 Å]. For $r\leq 3.25$ Å, the experimental PDFs and the $g_x(r)$ functions are in remarkable agreement, indicating that the distributions of distances between first neighbors are the same in BTZ relaxors and in the end-member compounds $BaTiO_3$ and $BaZrO_3$.

$$[\rho_0\bar{b}^2]_{BTZ}\times g_x(r)=(1-x)[\rho_0\bar{b}^2]_{BT}\times g_{BT}^{exp}(r)+x[\rho_0\bar{b}^2]_{BZ}\times g_{BZ}^{exp}(r), \quad (5)$$

where $g_{BT}^{exp}(r)$ and $g_{BZ}^{exp}(r)$ refer to the experimental PDFs of $BaTiO_3$ and $BaZrO_3$, respectively.

The experimental PDFs of BTZ relaxors ($x=0.25,0.32,0.35$) are compared with the corresponding $g_x(r)$ functions in Fig. 4. For all the studied compositions, a remarkable agreement is found in the r range [1.65–3.25 Å] that corresponds to the Ti-O, Zr-O, Ba-O, and O-O interatomic distances. Hence, the distributions of distances between the closest neighbors remain unchanged in BTZ relaxors with respect to $BaTiO_3$ and $BaZrO_3$, within the accuracy of the experiment. This observation implies that the bonds between the closest neighbors are rigid and almost not sensitive to the Ti/Zr substitution. Besides, the $g_x(r)$ function poorly reproduces the experimental PDF beyond 3.25 Å,

which indicates that the chemical substitution does influence the pair arrangements at larger scales.

The Ti-O (Zr-O) and O-O distance distributions are related to the structure of the TiO_6 (ZrO_6) octahedra, even if they do not allow a complete description of these octahedra in three dimensions. The similarity of the Ti-O and Zr-O distance distributions in the BTZ relaxors and in the end-member compounds $BaTiO_3$/$BaZrO_3$ thus suggests that the TiO_6 and ZrO_6 octahedra are similar in BTZ relaxors and in the end members, concerning both the Ti/Zr displacements and the deformation of the O_6 cages.

IV. TiO_6 AND ZrO_6 OCTAHEDRA IN $BaTiO_3$ AND $BaZrO_3$

In this section, the Ti-O and Zr-O distance distributions in $BaTiO_3$ and $BaZrO_3$ are analyzed in details. From the conclusions already obtained in Sec. III B, their description will be directly transferable to the case of BTZ relaxors, which is discussed in Sec. V.

In $BaZrO_3$, the local structure coincides with the crystallographic $Pm\bar{3}m$ perovskite structure, which leads to the conclusion that the Zr atoms lie at the center of regular oxygen octahedra, with a Zr-O distance equal to 2.096 Å. In $BaTiO_3$, the results obtained in Sec. III A show that it is necessary to analyze further the Ti-O distance distribution in order to describe the structure of the TiO_6 octahedra. This can be done by using the partial radial distribution function (RDF), $RDF_{Ti\to O}(r)$, which gives the average number of O atoms at the distance r from a Ti atom. Besides, the partial radial distribution function of Zr-O pairs in $BaZrO_3$ $RDF_{Zr\to O}(r)$ will also be considered to be used as a reference.

The partial RDF can be expressed as:[46]

$$\mathrm{RDF}_{\alpha\to\beta}(r) = \frac{1}{Nc_\alpha} \sum_{\substack{i_\alpha, i_\beta \\ i_\alpha \neq i_\beta}}^{N_\alpha, N_\beta} \langle \delta(r - |\vec{r_{i_\alpha}} - \vec{r_{i_\beta}}|) \rangle \tag{6}$$

$$= 4\pi r^2 \rho_0 c_\beta g_{\alpha\beta}(r) \tag{7}$$

In the latter equation, $g_{\alpha\beta}(r)$ is the α-β partial pair distribution function. According to the Faber-Ziman decomposition, it is related to the total pair distribution function, following:[46]

$$g(r) = \frac{1}{\bar{b}^2} \sum_{\alpha,\beta}^{n} c_\alpha c_\beta \overline{b_\alpha b_\beta} g_{\alpha\beta}(r). \tag{8}$$

The determination of $g_{\alpha\beta}(r)$ in the full r-range requires multiple measurements on samples with varying isotopic compositions.[46] However, in the present case, the objective is restricted to the determination of the distributions of Ti-O and Zr-O distances within the octahedra, and a simpler approach can be used. From the calculations presented in Sec. III A, all the Ti-O pairs (Zr-O pairs) contribute to the $g(r)$ of $BaTiO_3$ ($BaZrO_3$) for $r \leq 2.40$ Å, all the other α-β pair contributions occurring at larger r values. Hence, the $RDF_{Zr\to O}(r)$ and $RDF_{Ti\to O}(r)$ functions can be readily obtained from the experimental $g(r)$ of $BaZrO_3$ and $BaTiO_3$, respectively, by using successively Eqs. (8) and (7).

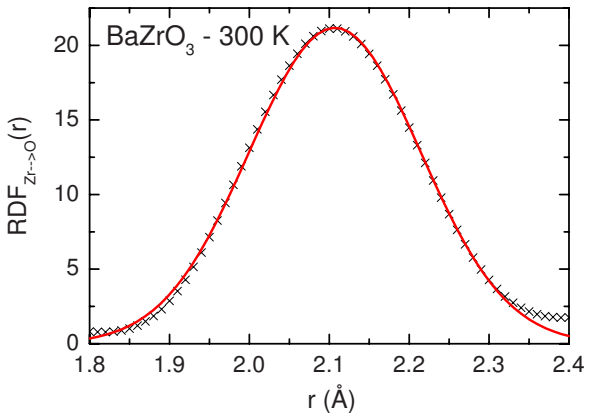

FIG. 5. (Color online) Experimental radial distribution function of Zr→O distances within the ZrO_6 octahedra in $BaZrO_3$ at 300 K (crosses). The solid line is a fit by a Gaussian peak (see text).

The $RDF_{Zr\to O}(r)$ and $RDF_{Ti\to O}(r)$ functions are represented in Figs. 5 and 6, in the r ranges [1.80–2.40 Å] and [1.65–2.40 Å], respectively. These bounds are chosen so that they correspond to minima of $|g(r)|$. The integrals of $RDF_{Ti\to O}(r)$ and $RDF_{Zr\to O}(r)$ in their respective r ranges are found equal to 5.5 and 5.7, respectively. Ideally, they should be equal to 6, the number of O atoms forming the octahedral cage around the Zr or Ti atoms. The measured values thus

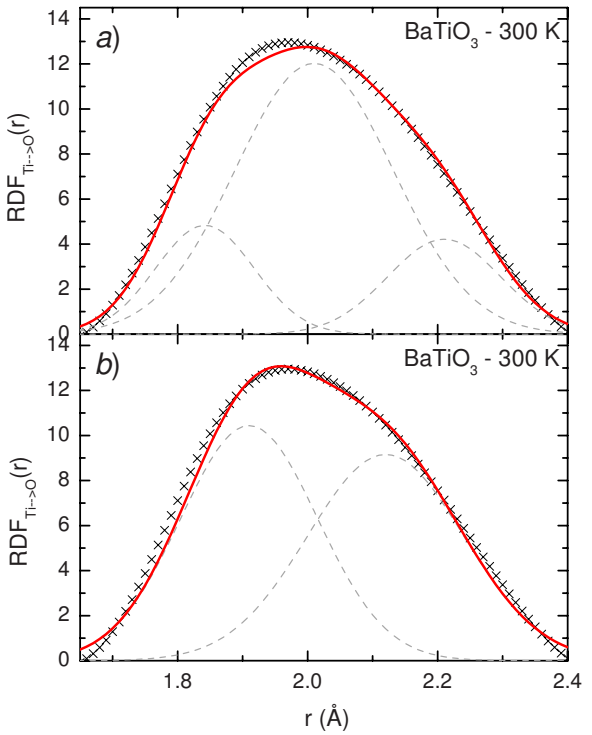

FIG. 6. (Color online) Experimental radial distribution function of Ti→O distances within the TiO_6 octahedra in $BaTiO_3$ at 300 K (crosses). The solid lines are fits within the hypothesis of (a) pure displacive phase transitions, and (b) pure order-disorder phase transitions (see text). Each group of Ti-O pairs with equal equilibrium lengths is assumed to lead to a Gaussian contribution to the RDF (dashed lines). The refined values of the positions and the mean-square deviations are reported in Table I.

TABLE I. Refined values of the parameters involved in the "purely displacive" and "purely order-disorder" models used to fit the radial distribution function of the Ti→O pair lengths within the TiO_6 octahedra in $BaTiO_3$ at 300 K. d_i is the position of the Gaussian peak associated with the ith pair length and σ_i^2 its mean-square deviation. The mean-square deviation of the ith pair length $[\sigma_{TiO}^2]_i$ is deduced from σ_i^2 by subtracting the width due to the data treatment (0.0076 ± 0.0010 Å^2). The uncertainties are of the order of ± 0.01 Å, ± 0.0005 Å^2, and ± 0.0015 Å^2 for d_i, σ_i^2, and $[\sigma_{TiO}^2]_i$, respectively.

			d_i (Å)	σ_i^2 (Å^2)	$[\sigma_{TiO}^2]_i$ (Å^2)
Purely displacive model	$i=1$	one short Ti-O distance	1.84	0.0057	−0.0019
	$i=2$	four intermediate Ti-O distances	2.01	0.0148	0.0072
	$i=3$	one long Ti-O distance	2.21	0.0075	−0.0001
Purely order-disorder model	$i=1$	three short Ti-O distances	1.91	0.0110	0.0034
	$i=2$	three long Ti-O distances	2.12	0.0144	0.0068

coincide with the expected one within an accuracy of 10%, which is standard for total scattering methods. The difference is mainly due to inadequacies in the choice of the integration r range in presence of unavoidable spurious oscillations of the RDF induced by the cutoff in Q space.

A. Zr-O pair RDF in $BaZrO_3$

In $BaZrO_3$, the Zr atoms lie at the center of regular oxygen octahedra, which creates 6 equal Zr-O distances. Assuming that the thermal atomic motions result in Gaussian distance distributions, the ideal $RDF_{Zr\rightarrow O}(r)$ [Eq. (6)] consists of a single Gaussian peak for $r \leqslant 2.40$ Å. For the experimental $RDF_{Zr\rightarrow O}(r)$, both the profile and the width are modified due to the limited Q range of the FT and the use of a weight function (Sec. II). Nevertheless, we tried to fit it by a Gaussian function in the r range [1.80–2.40 Å]. The area of the fitted peak was fixed to 5.7, which corresponds to the experimental area in that range. Both its position d and its mean-square deviation σ^2 were refined. Figure 5 shows that the experimental and fitted contributions are in excellent agreement. The fitted Zr-O distance, $d=2.105 \pm 0.010$ Å, is consistent with the one deduced from the crystallographic structure (2.096(1) Å). The refined value of the mean-square deviation $\sigma^2=0.0115(5)$ Å^2 includes the intrinsic Zr-O distance mean-square deviation (σ_{ZrO}^2) and the FT truncation effects. From a previous EXAFS study of $BaZrO_3$ at 300 K at the Zr K edge,[20] σ_{ZrO}^2 can be evaluated to 0.0039(5) Å^2. Hence, the mean-square deviation induced by the FT truncation effects can be estimated to $\sigma^2-\sigma_{ZrO}^2 = 0.0076 \pm 0.0010$ Å^2.

In conclusion, the analysis of the experimental $RDF_{Zr\rightarrow O}(r)$ shows that at $r \sim 2$ Å, the contribution of each interatomic distance to the experimental RDF can be described as a Gaussian peak within a good approximation, the contribution of the FT truncation effects to the mean-square deviation being equal to 0.0076 Å^2. This result will be used in the analysis of the experimental $RDF_{Ti\rightarrow O}(r)$.

B. Ti-O pair RDF in $BaTiO_3$

In $BaTiO_3$, the structure of the TiO_6 octahedra has been discussed intensely in the framework of the displacive and order-disorder models for the phase transitions.[7–11,47,48] In the low-temperature rhombohedral phase of $BaTiO_3$, it is admitted that each Ti atom is displaced from the center of its octahedron toward the $[111]_p$ direction in the pseudocubic perovskite cell. Locally, this displacement creates three short and three long Ti-O distances inside the octahedron ("3-3" distance distribution). When considering a pure displacive phase transition, the tetragonal structure at 300 K results from the reorientation of all the Ti displacements along the $[001]_p$ direction. In this case, the local structure around the Ti atoms corresponds to the crystallographic structure: inside each octahedron, the Ti displacement creates one short Ti-O distance, four intermediate Ti-O distances, and one long Ti-O distance ("1-4-1" distance distribution). In the case of a pure order-disorder phase transition, the tetragonal structure at 300 K results from the occupation of four equivalent sites that correspond to Ti displacements along the $[111]_p$, $[\bar{1}11]_p$, $[1\bar{1}1]_p$, and $[\bar{1}\bar{1}1]_p$ directions. Locally, the Ti displacement in its octahedron is then the same as in the low-temperature rhombohedral phase, resulting in a "3-3" distribution of the Ti-O distances.

It has already been noticed in Sec. III A that the Ti-O contribution to the experimental PDF differs from the one calculated in the tetragonal crystallographic structure ("1-4-1" distance distribution). In a first step, it is important to check whether this discrepancy is really due to the use of an nonsuitable distribution of the Ti-O distances, or due to the choice of inadequate hypotheses to calculate their mean-square deviations. For that purpose, three Gaussian peaks with independent mean-square deviations σ_i^2 $(i=1,2,3)$ were fitted to the experimental $RDF_{Ti\rightarrow O}(r)$ of $BaTiO_3$, in the r range [1.65–2.40 Å]. The relative weights of the peaks are 1, 4, and 1, the total area being fixed to 5.5, which corresponds to the experimental area. All the peak positions d_i $(i=1,2,3)$ were refined. The intrinsic mean-square deviations of the d_i distances, denoted $[\sigma_{TiO}^2]_i$, were estimated by subtracting 0.0076 Å^2 to the refined σ_i^2, according to the results obtained for the Zr-O pairs in $BaZrO_3$ (Sec. IV A). The values obtained for the d_i, σ_i^2, and $[\sigma_{TiO}^2]_i$ parameters are reported in Table I. As can be seen in Fig. 6(a), a good agreement can be obtained between the fitted and experimen-

tal RDFs, but with a negative value for $[\sigma^2_{TiO}]_1$ and a null one for $[\sigma^2_{TiO}]_3$, which is not physically acceptable. Moreover, fixing the $[\sigma^2_{TiO}]_1$ and $[\sigma^2_{TiO}]_3$ parameters to any positive values considerably alters the quality of the fit. In conclusion, the experimental RDF is not compatible with the hypothesis of a "1-4-1" distribution of the Ti-O distances within the TiO_6 octahedra in $BaTiO_3$, which means that the Ti atoms are not located on the fourfold tetragonal axis. This is in agreement with the results of a few previous structural studies of $BaTiO_3$,[9–11] including the room-temperature polarized x-ray absorption near-edge structure study at the Ti *K* edge by Ravel *et al.*[11]

In order to test the hypothesis of a "3-3" distribution of the Ti-O distances, two Gaussian peaks of area 5.5/2 were fitted to the experimental $RDF_{Ti\rightarrow O}(r)$ of $BaTiO_3$, in the *r* range [1.65–2.40 Å]. The positions of the peaks d_i and their mean-square deviations σ_i^2 $(i=1,2)$ were refined. Then, the intrinsic mean-square deviations of the d_i distances $[\sigma^2_{TiO}]_i$ were estimated by subtracting 0.0076 $Å^2$ to σ_i^2. The values of d_i, σ_i^2, and $[\sigma^2_{TiO}]_i$ are given in Table I. As shown in Fig. 6(b), a very good agreement between the fitted and experimental RDFs is achieved. The values obtained for $[\sigma^2_{TiO}]_1$ (0.0034 $Å^2$) and $[\sigma^2_{TiO}]_2$ (0.0068 $Å^2$) are reasonable for thermal motions at 300 K. At first sight, the large difference between $[\sigma^2_{TiO}]_1$ and $[\sigma^2_{TiO}]_2$ may appear to be surprising. In fact, the formation of short Ti-O bonds in $BaTiO_3$ was shown to be due to a hybridization of the Ti 3*d* and O 2*p* states within TiO_6 octahedra.[49] The short Ti-O bonds, which are partially covalent, are hence expected to be more rigid than the long ones, which could explain the difference between $[\sigma^2_{TiO}]_1$ and $[\sigma^2_{TiO}]_2$. Furthermore, a similar observation was reported for the Nb-O distances in the rhombohedral and orthorhombic phases of $KNbO_3$.[29,50,51] The $RDF_{Ti\rightarrow O}(r)$ of $BaTiO_3$ at 300 K is thus compatible with a "3-3" distribution of the Ti-O distances, which corresponds to a displacement of the Ti atoms in $[111]_p$ directions. However, note that the *r* resolution of the RDFs is not sufficient to distinguish a true "3-3" distribution of Ti-O distances from a similar but more complex distribution such as that proposed in Ref. 11. Given this fact, we can only conclude that the Ti atoms are located near the threefold axes of the pseudocubic perovskite cell in $BaTiO_3$ at 300 K (i.e., their position is shifted from the center toward one of the eight faces of the oxygen octahedra). Another important point is that the PDF method provides an average of instant snapshots of the local structure. Therefore, we cannot decide whether the average position of the Ti atoms is an equilibrium position (found in the case of localized harmonic motions) or not (in presence of more complex dynamical processes). That is to say, even though we found a "3-3" distribution of the Ti-O distances in $BaTiO_3$ at 300 K, we cannot directly conclude on the order-disorder character of its phase transitions.

The refined values for the three short and three long Ti-O distances in $BaTiO_3$ at 300 K are equal to 1.91(1) and 2.12(1) Å (Table I). It is interesting to compare these two lengths with those in the rhombohedral phase of $BaTiO_3$ at 15 K. In the latter case, the local and crystallographic structures coincide[7,8] so that the two Ti-O lengths at 15 K can be deduced from the diffraction study presented in Ref. 6: 1.878 and 2.135 Å. These values are close to those measured in the tetragonal phase at 300 K. Nevertheless, small differences exist. They cannot be due to thermal dilatation effects, which are of the order of 10^{-3} Å only.[6] We ascribe them to slight modifications of the Ti environment, which could be static (evolution of the structure of the TiO_6 octahedra) and/or dynamic (evolution of the Ti motions in their octahedral cages).

Neglecting these small differences, a rough estimation of the amplitude of the Ti displacement in $BaTiO_3$ at 300 K can be deduced from the structure of the TiO_6 octahedra at 15 K. From Ref. 6, at 15 K the Ti atoms are displaced from the center of deformed octahedra by 0.184 Å (in the $[111]_p$ direction). Hence, one can conclude that in $BaTiO_3$ at 300 K, the Ti displacement toward one face of its octahedron has an amplitude of approximately 0.18 Å.

Note that the PDF of $BaTiO_3$ at 300 K was previously reported in Ref. 29, but the presence of large spurious oscillations prevented any accurate description of the Ti-O distance distribution. Another way of measuring the Ti-O distances is to analyze the EXAFS at the Ti *K* edge. Unfortunately, the accuracy of this method is considerably lowered in the case of $BaTiO_3$ due to the presence of the Ba L_{III} edge which limits the available energy range.[11,52] Hence, to our knowledge, the present work provides the first estimation of the Ti-O distances and their mean-square deviations in $BaTiO_3$ at 300 K.

V. CONCLUDING DISCUSSION

This section is devoted to the structure of TiO_6 and ZrO_6 octahedra in BTZ relaxors and its possible implications on the relaxor behavior. According to the conclusions of Sec. III B, the distance distributions inside TiO_6 (ZrO_6) octahedra are identical, within the experimental accuracy, in BTZ relaxors and in $BaTiO_3$ ($BaZrO_3$). In the two following paragraphs, we begin with discussing the cation displacements and the octahedra dimensions in BTZ relaxors by using the results of Sec. IV.

The first result of the present work is that the Ti displacements present in the classical ferroelectric $BaTiO_3$ (~0.18 Å toward a face of the oxygen octahedra) persist in the BTZ relaxors, despite the Ti/Zr substitution on the octahedral site. The local dipole moments associated with the Ti^{4+} cations are thus similar in these two materials, although their dielectric properties strongly differ. No Zr displacements are found in BTZ relaxors, as it is the case in the paraelectric $BaZrO_3$. However, note that a previous EXAFS study at the Zr *K* edge[20] showed that the Zr-O distances at equilibrium are slightly more dispersed in BTZ relaxors than in $BaZrO_3$. If ascribed to a displacement of the Zr atoms within their oxygen cage, this disorder would correspond to a displacement smaller than 0.05 Å. In the present study, the accuracy of the distance distributions is limited by the superposition of the Ti-O and Zr-O contributions on the PDFs of BTZ relaxors, which impedes such an observation. In any case, the amplitude of the Ti^{4+} cation displacements is found to be much larger than the amplitude of the Zr^{4+} cation displacements in BTZ relaxors: the local polarization is thus mainly due to the Ti^{4+} cations.

The second conclusion of the present work is that the TiO_6 (ZrO_6) octahedra keep the same dimensions in BTZ relaxors and in $BaTiO_3$ ($BaZrO_3$), showing a very rigid character despite their large difference in size: the mean Ti-O distance is equal to 2.02 Å, while the Zr-O distance is equal to 2.10 Å. The BTZ relaxor structure is thus strongly distorted on the octahedra's scale. Of course, a superposition of perfectly rigid TiO_6 and ZrO_6 octahedra with different sizes is not compatible with the construction of a perovskite structure: the octahedra must be slightly distorted when put together. However, due to their limited r resolution, the PDFs do not allow to detect such distortions.

It is interesting to compare the results of the present work with those obtained from x-ray absorption or PDF studies of $CaTi_{1-x}Zr_xO_3$ (CTZ) (Refs. 53 and 54) and $PbTi_{1-x}Zr_xO_3$ (PZT),[21,34,55] which exhibit the same Ti/Zr substitution as BTZ relaxors but different dielectric properties. First, it is striking to note that in both CTZ and PZT, the measured Ti-O and Zr-O distances are different and tend to remain equal to the Ti-O and Zr-O distances measured in the end-member compounds.[34,53,55] In these systems such as in BTZ, the TiO_6 and ZrO_6 octahedra thus form rigid units. The analysis of x-ray absorption spectra and PDFs also provides interesting results on the atomic displacements. In CTZ, the Ti and Zr atoms were shown to lie at the center of their octahedra,[53,54] as it is the case in the $CaTiO_3$ and $CaZrO_3$ compounds.[56,57] In PZT, both the Ti and Zr atoms were found to be displaced in their octahedra,[21,55] while $PbTiO_3$ and $PbZrO_3$ exhibit ferroelectric and antiferroelectric instabilities, respectively.[58,59] Similarly with the BTZ system, the TiO_6 and ZrO_6 octahedra in CTZ and PZT thus present the same polar (or nonpolar) character as in their respective end members. One can propose that in the substituted $ATi_{1-x}Zr_xO_3$ perovskites (A=Ca, Ba, or Pb), the TiO_6 and ZrO_6 octahedra are rigid constituents, whose size and polar character are directly transferred from the end-member compounds $ATiO_3$ and $AZrO_3$.

The similarity of the local dipole moments in the classical ferroelectric $BaTiO_3$ and in BTZ relaxors is a key point of our results since it shows that the difference in the dielectric properties of these two materials only lies in different correlations between the cation displacements. According to models proposed earlier for "$BaTiO_3$-based" relaxors,[26,60] the Zr atoms would act as dilatational centers in BTZ relaxors, generating random electric fields[61] which in turn would favor the appearance of polar nanoregions. By giving evidence for structural distortions arising from the Ti^{4+}/Zr^{4+} difference in size, the present work shows that the latter models could actually explain the occurrence of the relaxor behavior in the BTZ solid solution. At first sight, they may appear insufficient since the local structural distortions found in BTZ relaxors are similar to those observed in the ferroelectric $PbTi_{1-x}Zr_xO_3$. However, one can first note that contrary to Ba atoms, Pb atoms largely get off the center of their oxygen cages in perovskite oxides due to a hybridization between the Pb 6p states and O 2p states.[62,63] Second, considering the substituted B site, only the Ti atoms are displaced in BTZ, while both Ti and Zr atoms are displaced in $PbTi_{1-x}Zr_xO_3$. Consequently, it seems reasonable to consider that the ferroelectric character would be more robust in $PbTi_{1-x}Zr_xO_3$ than in BTZ against random electric fields caused by the structural distortions.

ACKNOWLEDGMENTS

We are indebted to H.E. Fischer (ILL) for his help during the experiment on D4, and to J. Kreisel for fruitful discussions.

[1] L. E. Cross, Ferroelectrics **76**, 241 (1987).
[2] L. E. Cross, Ferroelectrics **151**, 305 (1994).
[3] A. A. Bokov and Z. G. Ye, J. Mater. Sci. **41**, 31 (2006).
[4] M. Pasciak, M. Wolcyrz, and A. Pietraszko, Phys. Rev. B **76**, 014117 (2007).
[5] J. Ravez and A. Simon, Eur. J. Solid State Inorg. Chem. **34**, 1199 (1997).
[6] G. H. Kwei, A. C. Lawson, S. J. L. Billinge, and S. W. Cheong, J. Phys. Chem. **97**, 2368 (1993).
[7] R. Comès, M. Lambert, and A. Guinier, Solid State Commun. **6**, 715 (1968).
[8] R. Comès, M. Lambert, and A. Guinier, Acta Crystallogr. A **26**, 244 (1970).
[9] B. Zalar, V. V. Laguta, and R. Blinc, Phys. Rev. Lett. **90**, 037601 (2003).
[10] B. Zalar, A. Lebar, J. Seliger, R. Blinc, V. V. Laguta, and M. Itoh, Phys. Rev. B **71**, 064107 (2005).
[11] B. Ravel, E. A. Stern, R. I. Vedrinskii, and V. Kraizman, Ferroelectrics **206**, 407 (1998).
[12] A. R. Akbarzadeh, I. Kornev, C. Malibert, L. Bellaiche, and J. M. Kiat, Phys. Rev. B **72**, 205104 (2005).
[13] I. Levin, T. G. Amos, S. M. Bell, L. Farber, T. A. Vanderah, R. S. Roth, and B. H. Toby, J. Solid State Chem. **175**, 170 (2003).
[14] M. D. Mathews, E. B. Mirza, and A. C. Momin, J. Mater. Sci. Lett. **10**, 305 (1991).
[15] S. F. Dec, M. F. Davies, G. E. Maciel, C. E. Bronnimann, J. J. Fitzgerald, and S. Han, Inorg. Chem. **32**, 955 (1993).
[16] J. S. Hartman, F. P. Koffyberg, and J. A. Ripmeester, J. Magn. Reson. (1969-1992) **91**, 400 (1991).
[17] D. Haskel, B. Ravel, M. Newville, and E. A. Stern, Physica B **208-209**, 151 (1995).
[18] L. A. Bugaev, V. A. Shuvaeva, I. B. Aleseenko, and R. V. Vedrinskii, Physica B **208-209**, 169 (1995).
[19] P. E. Petit, F. Guyot, and F. Farges, J. Phys. IV **7C2**, 1065 (1997).
[20] C. Laulhé, F. Hippert, J. Kreisel, M. Maglione, A. Simon, J. L. Hazemann, and V. Nassif, Phys. Rev. B **74**, 014106 (2006).
[21] R. V. Vedrinskii, E. S. Nazarenko, M. P. Lemeshko, V. Nassif, O. Proux, A. A. Novakovich, and Y. Joly, Phys. Rev. B **73**, 134109 (2006).
[22] R. D. Shannon, Acta Crystallogr., Sect. A: Cryst. Phys., Diffr., Theor. Gen. Crystallogr. **32**, 751 (1976).

[23] T. N. Verbitskaia, G. S. Zhdanov, I. N. Venevstev, and S. P. Soloviev, Sov. Phys. Crystallogr. **3**, 182 (1958).
[24] P. Sciau, G. Calvarin, and J. Ravez, Solid State Commun. **113**, 77 (2000).
[25] V. Westphal, W. Kleemann, and M. D. Glinchuk, Phys. Rev. Lett. **68**, 847 (1992).
[26] R. Farhi, M. El Marssi, A. Simon, and J. Ravez, Eur. Phys. J. B **18**, 605 (2000).
[27] T. Egami and S. J. L. Billinge, *Underneath the Bragg Peaks-Structural Analysis of Complex Materials* (Pergamon, New York, 2003).
[28] H. D. Rosenfeld and T. Egami, Ferroelectrics **164**, 133 (1995).
[29] G. H. Kwei, S. J. L. Billinge, S. W. Cheong, and J. G. Saxton, Ferroelectrics **164**, 57 (1995).
[30] S. Teslic, T. Egami, and D. Viehland, Ferroelectrics **194**, 271 (1997).
[31] S. Teslic and T. Egami, Acta Crystallogr., Sect. B: Struct. Sci. **54**, 750 (1998).
[32] T. Egami, W. Dmowski, M. Akbas, and P. K. Davies, AIP Conf. Proc. **436**, 1 (1998).
[33] W. Dmowski, M. K. Akbas, P. K. Davies, and T. Egami, J. Phys. Chem. Solids **61**, 229 (2000).
[34] W. Dmowski, T. Egami, L. Farber, and P. K. Davies, AIP Conf. Proc. **582**, 33 (2001).
[35] P. Juhas, I. Grinberg, A. M. Rappe, W. Dmowski, T. Egami, and P. K. Davies, Phys. Rev. B **69**, 214101 (2004).
[36] I. K. Jeong, J. K. Lee, and R. H. Heffner, Appl. Phys. Lett. **92**, 172911 (2008).
[37] C. L. Farrow, P. Juhas, J. W. Liu, D. Bryndin, E. S. Božin, J. Bloch, Th. Proffen, and S. J. L. Billinge, J. Phys.: Condens. Matter **19**, 335219 (2007).
[38] M. G. Tucker, D. A. Keen, M. T. Dove, A. L. Goodwin, and Q. Hui, J. Phys.: Condens. Matter **19**, 335218 (2007).
[39] H. E. Fischer, G. J. Cuello, P. Palleau, D. Feltin, A. C. Barnes, Y. S. Badyal, and J. M. Simonson, Appl. Phys. A: Mater. Sci. Process. **74**, S160 (2002).
[40] H. H. Paalman and C. J. Pings, J. Appl. Phys. **33**, 2635 (1962).
[41] I. A. Blech and B. L. Averbach, Phys. Rev. **137**, A1113 (1965).
[42] J. L. Yarnell, M. J. Katz, R. G. Wenzel, and S. H. Koenig, Phys. Rev. A **7**, 2130 (1973).
[43] K. Sköld and D. L. Price, *Methods of Experimental Physics* Vol. 23, (Academic, New York, 1986).
[44] The choice of this Gaussian function is known to reduce the magnitude of the secondary oscillations without leading to a prohibitive supplementary broadening of the main one (see [B. Warren, *X-ray diffraction* (Dover, New York, 1991)]).
[45] A r-dependence of the mean-square deviation of the interatomic distances has to be introduced for each type of atomic pairs, in order to take into account the correlations between the closest-neighbor thermal motions (see [I. K. Jeong, T. Proffen, F. Mohiuddin-Jacobs, and S. J. L. Billinge, J. Phys. Chem. A **103**, 921 (1999)] and references therein). The relative thermal motions of two atoms are governed by their bond type, and hence are different in each material. Here, the choice of Eq. (4) as an expression of $\sigma^2_{\alpha\beta}(r)$ allows to optimize the agreement between the experimental PDF of the reference compound $BaZrO_3$ and the PDF calculated from its crystallographic structure.
[46] H. E. Fischer, A. C. Barnes, and P. S. Salmon, Rep. Prog. Phys. **69**, 233 (2006).
[47] A. Hüller, Solid State Commun. **7**, 589 (1969).
[48] E. A. Stern, Phys. Rev. Lett. **93**, 037601 (2004).
[49] R. E. Cohen, Nature (London) **358**, 136 (1992).
[50] N. de Mathan, E. Prouzet, E. Husson, and H. Dexpert, J. Phys.: Condens. Matter **5**, 1261 (1993).
[51] A. I. Frenkel, F. M. Wang, S. Kelly, R. Ingalls, D. Haskel, E. A. Stern, and Y. Yacoby, Phys. Rev. B **56**, 10869 (1997).
[52] B. Ravel, C. E. Bouldin, H. Renevier, J.-L. Hodeau, and J.-F. Berar, Phys. Rev. B **60**, 778 (1999).
[53] I. Levin, E. Cockayne, M. W. Lufaso, J. C. Woicik, and J. E. Maslar, Chem. Mater. **18**, 854 (2006).
[54] V. Krayzman, I. Levin, J. C. Woicik, D. Yoder, and D. A. Fischer, Phys. Rev. B **74**, 224104 (2006).
[55] D. Cao, I. K. Jeong, R. H. Heffner, T. Darling, J. K. Lee, F. Bridges, J. S. Park, and K. S. Hong, Phys. Rev. B **70**, 224102 (2004).
[56] H. J. A. Koopmans, G. M. H. van de Velde, and P. J. Gellings, Acta Crystallogr., Sect. C: Cryst. Struct. Commun. **39**, 1323 (1983).
[57] S. Sasaki, C. T. Prewitt, and J. D. Bass, Acta Crystallogr., Sect. C: Cryst. Struct. Commun. **43**, 1668 (1987).
[58] R. J. Nelmes and W. F. Kuhs, Solid State Commun. **54**, 721 (1985).
[59] A. M. Glazer, K. Roleder, and J. Dec, Acta Crystallogr., Sect. B: Struct. Sci. **49**, 846 (1993).
[60] V. V. Shvartsman, W. Kleemann, J. Dec, Z. K. Xu, and S. G. Lu, J. Appl. Phys. **99**, 124111 (2006).
[61] M. D. Glinchuk and I. V. Kondakova, Solid State Commun. **96**, 529 (1995).
[62] D. J. Singh, Phys. Rev. B **73**, 094102 (2006).
[63] M. Suewattana and D. J. Singh, Phys. Rev. B **73**, 224105 (2006).